Structure of the stochastic layer of a perturbed resonant triad

Miroslaw Latka and Bruce J. West
Center for Nonlinear Science and Department of Physics, University of North Texas, P.O. Box 5368, Denton, Texas 76203
(Received 24 April 1995)

We have studied the interaction of capillary wave resonant triads with a gravity wave. The isolated resonant triad is integrable but when perturbed by the longer wavelength gravity wave the corresponding Hamiltonian dynamics becomes nonintegrable. We have derived the separatrix mapping which well approximates the dynamics in the vicinity of the separatrix. With the help of this mapping we analyze the structure of the stochastic layer of the driven resonant triad.

PACS number(s): 47.20.Ky, 47.52.+j, 05.45.+b, 47.10.+g

In many physical systems weak anharmonicities can give rise to a variety of nonlinear interactions. Nonlinear *resonant* interactions are particularly important in Hamiltonian systems since they provide a mechanism for energy transfer among modes belonging to given resonant groups [1–3]. In the theory of nonlinear waves the lowest order nonlinear resonant interaction may occur for three waves with frequencies Ω_i $(i = 1, 2, 3)$ and corresponding wave vectors $\mathbf{k}_i$ which satisfy the following conditions: $\Omega_1 = \Omega_2 \pm \Omega_3$ and $\mathbf{k}_1 = \mathbf{k}_2 \pm \mathbf{k}_3$. The waves which match these conditions are often referred to as *resonant triads.*

Examples of three-wave interaction may be drawn from quite diverse fields ranging from nonlinear optics, plasma physics to stimulated Raman and Brillouin scattering (see, e.g., [4] and references therein). In geophysical fluid dynamics resonant triads can occur for three gravity-capillary waves [5], three internal waves [6,7], and two surface gravity waves coupled to a single internal wave [8,9].

The criterion for the stability of such resonant triad interactions was given by Hasselmann [10]. He showed that the nonlinear coupling between two infinitesimal amplitude waves and a finite amplitude wave in resonance is unstable for the sum interaction and neutrally stable for the difference interaction. Herein, we extend that analysis to determine the global stability of resonant triads using Hamiltonian dynamical techniques. In particular, we examine the breakup of Kolmogorov-Arnold-Moser (KAM) tori present in the isolated triad and the formation of a stochastic layer due to external periodic perturbations.

In this paper we discuss the transition to chaos in a one-dimensional, time dependent Hamiltonian which describes the dynamics of a resonant triad of three short gravity-capillary waves riding atop a longer gravity wave [11,12]: $H = H_0 - \gamma j \cos \omega t$, where the Hamiltonian H_0 of the isolated triad may be written as $H_0 = \sqrt{j(1-j)(j+j^*)}\sin\psi$. The harmonic perturbation in the Hamiltonian H models the coupling between the long wavelength gravity wave and the resonant triad. In the linear approximation of this interaction, considered herein, the gravity wave acts as an external driver and is not influenced by the resonant triad. The dimensionless wave action j and canonically conjugate phase ψ may be directly related to mode amplitudes via a sequence of canonical transformations, and the constant j^* measures the asymmetry in wave action between the two longer waves in the triad.

The phase space portrait of an isolated triad shown in Fig. 1, periodic in the variable ψ with period 2π, is made up of cells of length π with alternating direction of rotations. The geometry of this phase space is reminiscent of that of two-dimensional Rayleigh-Bénard convection [13]. The small filled rectangles at the edges of the cells represent degenerate hyperbolic fixed points $p_n^{\pm} = (n\pi, \pm 1)$. The dashed lines in Fig. 1 denote the heteroclinic orbits which connect the unstable hyperbolic fixed points and form a separatrix. The vertical branches of the separatrix (connecting fixed points p_n^+ and p_n^-) delineate the regions of phase space with different directions of rotation. The separatrices enclose the stable elliptic fixed points located at $(n\pi/2, 2/3)$, and these fixed points are depicted in Fig. 1 by the filled circles.

The dynamics of the isolated triad is integrable. The time evolution of the wave action j, important in subsequent discussion, may be written as [14]

$$j(t) = j_3 - (j_3 - j_2)\mathrm{sn}^2[\tfrac{1}{2}\sqrt{j_3 - j_1}(t - t_0)], \qquad (1)$$

where sn is the Jacobi sine function and j_1, j_2, j_3 are the roots of the equation $j^2(1-j) = E^2$ arranged in the ascending order $j_1 \le j_2 < j_3$. E is the dimensionless energy of the unperturbed motion ($|E| <= E_{max} = 2/(3\sqrt{3})$.

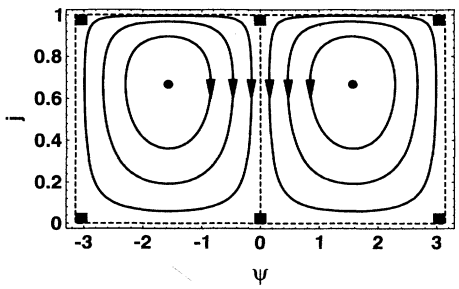

FIG. 1. The phase space portrait of the isolated resonant triad with $j^* = 0$. The filled circles and rectangles show the position of the elliptic and hyperbolic fixed points, respectively. The box shaped separatrix (dashed lines) delineates the regions of phase space with different direction of motion.

The period of rotation is given by

$$T = \frac{4K(m)}{\sqrt{j_3 - j_1}}, \qquad m = \sqrt{\frac{j_3 - j_2}{j_3 - j_1}}, \tag{2}$$

$K(m)$ is the complete elliptic integral of the first kind and m is its amplitude. For $E = 0$ the motion takes place along the separatrix ($m = 1$, $T = \infty$). For the vertical heteroclinic orbit connecting the fixed points p_n^+ and p_n^- (1) reduces to the following form:

$$j_{sx}(t) = \operatorname{sech}^2[\tfrac{1}{2}(t - t_0)]. \tag{3}$$

When the resonant triad is affected by the harmonic perturbation the stable and unstable manifolds associated with the hyperbolic fixed points transversely intersect in the extended phase space. This intersection leads to the destruction of the separatrix and the formation of a stochastic layer. Note that any trajectory within the chaotic layer is no longer confined to a particular cell but in the course of time may migrate to other cells. The occurrence of the transversal intersection may be explicitly shown by calculating the Melnikov function $M(t_0)$ [16,17,13] which is a measure of the distance between the stable and unstable manifolds at a given instant. Here, using the separatrix solution (3) for the resonant triad we obtain

$$M(t_0) = \gamma \int_{-\infty}^{\infty} \frac{dj_{sx}}{dt} \cos(\omega t) dt = -\frac{4\gamma\pi\omega^2 \sin \omega t_0}{\sinh \pi\omega}. \tag{4}$$

The formation of the heteroclinic tangle which follows the transversal intersection takes place whenever $M(t_0)$ changes sign. This passage through zero is trivially guaranteed by the form of the above equation.

The regular and chaotic motion near the separatrix of nonlinear systems may be studied with the help of the *separatrix* or *whisker* mapping originally introduced by Chirikov [1] to analyze the dynamics of the pendulum. The derivation of this type of twist mapping for the resonant triad is based upon the specific behavior of the wave action j in unperturbed motion in the vicinity of the separatrix. In Fig. 2 we display the time evolution of j for a typical trajectory close to the separatrix ($|E| \ll E_{max}$). Interestingly enough, the width of the wave action pulses for orbits with low absolute energies only weakly depends on the energy and is well approximated by the period of small oscillations T_0 around the elliptic fixed points from

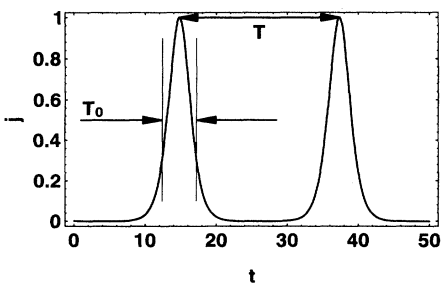

FIG. 2. Time evolution of wave action j for a typical trajectory in the neighborhood of the separatrix.

Fig. 1. The spacing between the pulses is equal to the period of motion $T(E)$ [cf. (2)]. This character of the dynamics of wave action j determines the response of the resonant triad to small perturbations. The change in the unperturbed energy of the triad induced by the gravity wave is given by

$$\frac{dH_0}{dt} = \{H_0, H\} = \frac{\partial H_0}{\partial \psi}\frac{\partial V}{\partial j} = \gamma \frac{dj}{dt}\cos(\omega t). \tag{5}$$

Thus as long as the perturbation does not destroy the characteristic functional form of the wave action $j(t)$ evolution (cf. Fig. 2) the effect of the driving should be confined to time intervals corresponding to the j peaks. This prediction is verified in Fig. 3 where the change in the unperturbed energy $E(t) - E(0)$ is superimposed with the evolution of the wave action. One can see that the rapid variation of the energy within a given pulse is followed by an interval during which the energy hardly changes. Since the period $T(E)$ of the unperturbed motion diverges as $E \to 0$, the closer a trajectory approaches the separatrix the greater the spacing between the j peaks and the longer the intervals during which the energy remains approximately constant. This observation constitutes the physical essence of the separatrix mapping.

The formal derivation of the whisker mapping involves the calculation of the change in unperturbed energy ΔE per period of motion in proximity to the separatrix. If we assume that a j pulse is centered at time t_n then using (5) we may write

$$\begin{aligned}\Delta E_n &= \gamma \int_{t_n - T/2}^{t_n + T/2} \frac{dj}{dt}\cos(\omega t) dt \\ &\approx \gamma \int_{-\infty}^{\infty} \frac{dj_{sx}}{dt}\cos[\omega(t + t_n)] dt.\end{aligned} \tag{6}$$

Following the standard procedure [1,15] we approximate ΔE_n by evaluating the integral in (6) on the unperturbed separatrix (cf. Fig. 1) rather than along the actual trajectory. Consequently, the limits of integrations are extended to plus and minus infinity. Note that only the vertical whiskers of the separatrix contribute to the above integral. The motion on these vertical heteroclinic orbits is parametrized in such a way that $j_{sx}(0) = 1$ [which is achieved by setting t_0 in Eq. (3) equal to zero]. The ac-

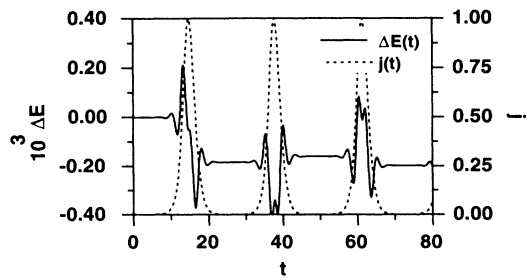

FIG. 3. Change in unperturbed energy $\Delta E = E(t) - E(0)$ for a trajectory from the vicinity of the separatrix is superimposed with the evolution of the wave action j to show that the effect of the external perturbation is determined by the character of the dynamics of the wave action ($\omega = 2$, $\gamma = 0.001$).

tual wave action pulse is peaked at time t_n so that we adjust the explicit time dependence of the perturbation in the above equation to $t+t_n$. One can see that the change in unperturbed energy is given by the absolute value of the Melnikov function $M(t_n)$ [cf. (4)] and since this function is dependent upon the phase of the perturbation it is convenient to use this phase to measure time. The change of phase between the successive j pulses n and $n+1$ is just $\omega T(E_{n+1})$ where $E_{n+1} = E_n + \Delta E_n$ is the plateau energy resulting from the nth kick [cf. Fig. 3]. In further analysis we replace the period of unperturbed motion (2) by the following formula valid for orbits in the vicinity of the separatrix ($m \approx 1$): $T(E) \approx 2\ln(8/E)$ (see [12] for the complete derivation and a discussion of its validity). Using this approximate period we may write the separatrix mapping for the resonant triad in the following form:

$$E_{n+1} = E_n + \frac{4\gamma\pi\omega^2 \sin\phi_n}{\sinh \pi\omega}, \tag{7}$$

$$\phi_{n+1} = \phi_n + 2\omega \ln \frac{8}{E_{n+1}}. \tag{8}$$

In Fig. 4(a) we present a simplified image of the portion of the phase space of the separatrix mapping with $\omega = 2$ and $\gamma = 0.001$. This figure reveals the formation of a stochastic layer bounded by the parts of the phase space where motion remains predominantly regular for this strength of perturbation. The structure of the regular region is strongly influenced by the presence of the prominent nonlinear resonance islands, known as KAM islands.

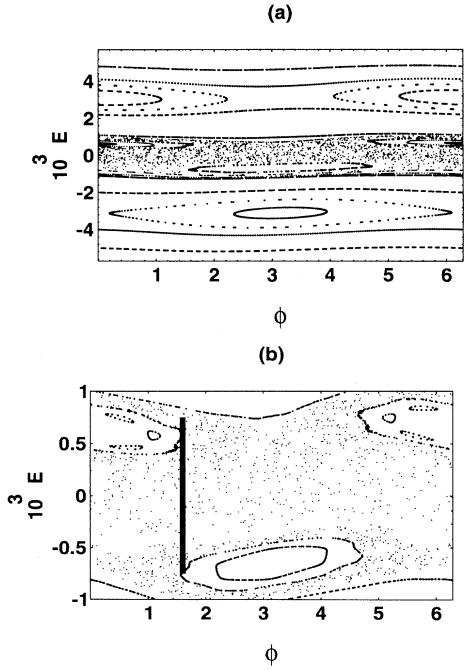

FIG. 4. (a) Separatrix mapping corresponding to the perturbed resonant triad ($\omega = 2$, $\gamma = 0.001$). (b) Magnification of the stochastic region from (a). The filled vertical bar represents the estimated width of the chaotic layer.

We have already mentioned that when a resonant triad is perturbed the trajectories belonging to the stochastic layer are no longer confined to a particular cell (cf. Fig. 1) but eventually wander into neighboring cells. We refer to such trajectories or their phases ψ as traveling or untrapped. The whisker mapping captures this feature of the dynamics of the driven resonant triad. Any trajectory launched from within the stochastic sea, enlarged in Fig. 4(b), under the action of the map moves erratically, occasionally crossing the line $E = 0$. This crossing, however, may be identified as a migration between adjacent cells since the sign of the unperturbed energy alternates between the cells.

The separatrix mapping also provides insight into the origin of the stochasticity of a weakly perturbed resonant triad. In the neighborhood of the elliptic fixed point the period of motion is weakly energy dependent. On the contrary, in the separatrix region the period of rotation T diverges and consequently a small variation of energy leads to a considerable change in the phase of the corresponding mapping. If we measure the stretching of a small phase interval $\delta\phi$ with the parameter $K = |\delta\phi_{n+1}/\delta\phi_n - 1|$ [15] then local instability occurs when $K \geq 1$. Employing equations (7) and (8) we may derive an approximation for the width of the stochastic layer: $|E| < 8\omega^3\gamma\pi/\sinh(\pi\omega)$. In Fig. 4(b) the filled vertical bar represents the width of the stochastic layer calculated using this formula. While this estimate is usually good, it cannot take into account the effect of the island chains or cantori immersed in the stochastic sea on the transport properties of the map [18].

The question arises as to how accurately the whisker mapping approximates the actual dynamics. Weiss and Knobloch [19] in their studies of the mass transport and mixing in modulated traveling waves found good agreement between the statistical properties of chaotic trajectories calculated with the help of the separatrix map with those obtained by the explicit numerical integration of Hamilton's equations of motion. However, the most direct assessment of the validity of the map is provided by the comparison of its phase space structure with that of the map determined numerically without invoking the typical approximations involved in the derivation of the separatrix map. Figure 5 shows an example of the latter mapping constructed for the same parameters as those

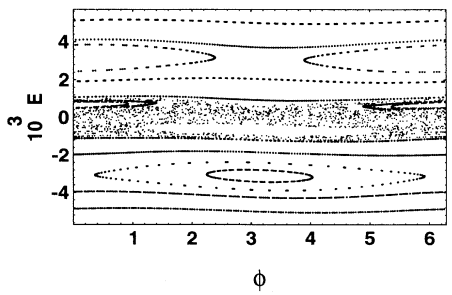

FIG. 5. Analog of whisker mapping constructed numerically without the approximations involved in derivation of the mapping [Eqs. (7) and (8)]. The model parameters are the same as those used in Fig. 4.

used in Fig. 4. For each phase space point in Fig. 5 we calculated the position t_n of the maximum of the wave action pulse and the plateau energy established after the perturbation kick associated with this pulse (cf. Fig. 3). Comparing Figs. 4(a) and 5 we can see that for this strength of perturbation the separatrix mapping well reproduces the position and width of the major nonlinear resonances and the stochastic layer. We emphasize that apart from the model specific coefficients the functional form of mapping [Eqs. (7) and (8)] is generic, which is to say that it describes motion in the vicinity of the separatrix of a large class of previously investigated Hamiltonian systems [1,15,18,19] as well as nonlinear wave-wave interactions studied herein.

In the future [12] we will apply the whisker map, derived in this work, to the study of the transport properties of a field of capillary wave resonant triads interacting with gravity waves. We will also discuss the influence of dynamical chaos on the statistics of the short scale structure of the ocean surface wave field.

This work was supported by the Office of Naval Research under Grant No. N00014-92-J-1604. The authors thank the National Science Foundation for support of the numerical calculations performed on the CRAY C90 at the Pittsburgh Supercomputing Center (Grant No. PHY920023P).

[1] B.V. Chirikov, Phys. Rep. **56**, 263 (1979).
[2] J.D. Meiss and K.M. Watson, *Topics in Nonlinear Dynamics*, edited by S. Jorna (AIP, New York, 1978), Vol. 46, p. 296.
[3] B.J. West, *Deep Water Gravity Waves (Weak Interaction Theory)*, Lecture Notes in Physics Vol. 146 (Springer-Verlag, Berlin, 1981).
[4] D.J. Kaup, Stud. Appl. Math. **55**, 93 (1976).
[5] O.M. Phillips, J. Fluid Mech. **9**, 193 (1960).
[6] J.D. Meiss, N. Pomphey, and K.M. Watson, Proc. Natl. Acad. Sci. USA **76**, 2109 (1979).
[7] *Nonlinear Properties of Internal Waves*, edited by B.J. West (AIP, New York, 1981).
[8] J.R. Alper, H.M. Byrne, J.R. Proni, and R.L. Chernell, J. Geophys. Res. **80**, 865 (1975).
[9] See papers in J. Geophys. Res. **80** (1975) for an extensive review.
[10] K.H. Hasselmann, J. Fluid Mech. **30**, 737 (1967).
[11] K. Trulsen and C.C. Mei, J. Fluid. Mech. **290**, 345 (1995).
[12] M. Latka and B.J. West (unpublished).
[13] S. Wiggins, *Chaotic Transport in Dynamical Systems* (Springer-Verlag, New York, 1992).
[14] A.D.D. Craik, *Wave Interactions and Fluid Flows* (Cambridge University Press, Cambridge, 1985).
[15] G.M. Zaslavsky, R.Z. Sagdeev, D.A. Usikov, and A.A. Chernikov, *Weak Chaos and Quasi-regular Patterns* (Cambridge University Press, Cambridge, 1991).
[16] K. Melnikov, Trans. Moscow Math. Soc. **12**, 1 (1963).
[17] A. Lichtenberg and M.A. Lieberman, *Regular and Stochastic Motion* (Springer-Verlag, New York, 1992).
[18] Y. Yamaguchi, Phys. Lett. **109A**, 191 (1985); Prog. Theor. Phys. **72**, 694 (1984).
[19] J.B. Weiss and E. Knobloch, Phys. Rev. A **40**, 2579 (1989).